Universal relaxation behavior of classical liquid crystals at hypersonic frequencies

C. Grammes,[1] J. K. Krüger,[1] K.-P. Bohn,[1] J. Baller,[1] C. Fischer,[1] C. Schorr,[1] D. Rogez,[2] and P. Alnot[3]
[1]*Experimentalphysik 10.2, Universität des Saarlandes, Postfach 151150, D-66041 Saarbücken, Germany*
[2]*Laboratoire d'Ultrasons et de Dynamique des Fluides Complexes, Université Louis Pasteur, Strasbourg, France*
[3]*Laboratoire Central de Recherche, Thomson CSF, F-91404 Orsay, Cedex, France*
(Received 31 May 1994)

Within this work we present comparative Brillouin and ultrasonic investigations of *p*-methoxybenzylidene *p*-(*n*-butylaniline), *p*-azoxyanisol, and 4-cyano-4'-pentyl-biphenyl performed in the vicinity of the nematic-isotropic transition. We confirm the existence of a universal hypersonic relaxation mechanism of weak activation energy and a related significant splitting of the two principal longitudinal acoustic modes within the nematic phase. Brillouin refractometry is proposed as a method to determine the magnitude of the nematic order parameter simultaneously with the second-order elastic stiffness constants. The origin of the hypersonic anisotropy is discussed in terms of thermal relaxations and the evolution of the nematic order parameter.

PACS number(s): 61.30.−v

I. INTRODUCTION

From the point of view of classical liquids and solids, nematic liquid crystals (NLCs) show a somewhat unexpected behavior concerning their second-order elasticity. Despite their considerable uniaxial molecular orientation, classical nematic liquid crystals show no static elastic anisotropy and no shear stiffness; this is a consequence of their fluidity and their continuously broken orientational symmetry [1,2]. In contrast to classical liquids and solids, NLC's show the so-called flex elasticity (director elasticity), which is generally discussed in terms of the Frank elastic constants [3]. The complete low frequency elastic properties including the degeneracy of the second-order elastic properties are well described by existing hydrodynamic theories [2,4–6]. Slight elastic anisotropies of the order of 10^{-3}, observed in several NLC's with alkylic chains as end groups, that were measured at ultrasonic frequencies could be explained in a satisfactory manner by intramolecular relaxation processes [5,7]. Bradberry and co-workers [8,9], Krüger [10], and Gleed, Sambles, and Bradberry [11] have shown that virtually all NLC's show a significant elastic anisotropy. First hints of a significant additional relaxation process at hypersonic frequencies were reported for *p*-methoxybenzylidene *p*-(*n*-butylaniline) (MBBA) (see Table I) by Clark and Liao [12]. However, its origin was not clear yet, although the idea was presented to interpret it in terms of a thermal relaxation process.

TABLE I. Chemical formulas of the investigated samples.

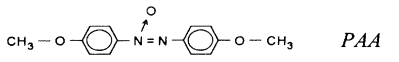	*PAA*
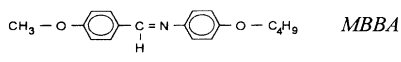	*MBBA*
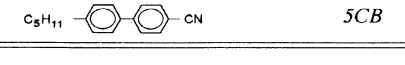	*5CB*

The aim of the present work is to confirm the existence of an additional relaxation process at hypersonic frequencies in nematic liquid crystals, to discuss its origin and its influence on sound mode propagation, and to point out its universality for all nematic liquid crystals. For this purpose we have investigated several NLC's belonging to three different chemical classes. We will discuss possible dispersion mechanisms including their effect on the phase and the group velocity. Moreover, we will demonstrate and discuss a correlation between the elastic anisotropy and the magnitude of the nematic order parameter.

As further experimental progress we propose the technique of Brillouin refractometry that allows the measurement of the optoacoustic dispersion function and of the birefringence of NLC's films. This technique is especially suitable for investigations of thin films of nematic liquid crystals. The optoacoustic dispersion function [10,13] has been used in this work to confirm the existence of the relaxation process mentioned above and to demonstrate that this process has only a weak activation energy. Brillouin refractometry yields a method to determine the magnitude of the nematic order parameter.

II. EXPERIMENT

A. Samples and sample preparation

In order to compare our results with those from literature we chose among others the frequently investigated materials MBBA and *p*-azoxyanisol (PAA) (Tables I and II). While PAA is a highly symmetric molecule with methylic end groups, the MBBA molecule has one butylic end group that provides some flexibility. Furthermore, in order to investigate the influence of the alkyl chains on the acoustic properties of NLC's, we selected a homolog of the class of 4-cyano-4-*n*-alkylbiphenyles (*n*-CB): 5CB. The phase behavior and nematic-isotropic transition temperatures T_{NI} of the investigated samples are given in Table II. The samples had been recrystallized before the

TABLE II. Phase sequences and transition temperatures (in K) of the investigated samples. Phases: cryst, crystalline; n, nematic; iso, isotropic.

Material	Phase sequence				
PAA	cryst.	391.2	n	408.7	iso
MBBA	cryst.	294.2	n	318.2	iso
5CB	cryst.	297.2	n	308.7	iso

measurements in order to avoid environmental influences, such as water adsorption, that could change the physical properties; for example, it causes a shift of T_{NI}.

All samples were prepared using surface treatment techniques [rubbed polyimide films (PIM)]. The PIM technique yields transparent and highly oriented NLC samples perfectly adapted to Brillouin investigations. A schematical drawing of a sandwich cell including an orthogonal sample coordinate system (x_1,x_2,x_3) is given in Fig. 1. Typical sample thicknesses extend from 25 to 75 μm. The x_3 direction has been chosen to be directed along the rubbing direction R of the PIM films; x_3 therefore defines the unique axis of the NLC samples and x_2 has been defined to be perpendicular to the film plane. Although the oriented sample area was about 10×10 mm^2, the investigated scattering volume extends only to a diameter of about 50 μm because of laser beam focusing onto the sample. In operating this way one may easily avoid artifacts due to sample defects.

B. High performance Brillouin spectroscopy

The details of the Brillouin spectrometer as well as of the applied techniques to evaluate information about the elastic and some of the optic properties of anisotropic samples are given elsewhere [13,14]. The main purpose of Brillouin spectroscopy is to obtain information about the hypersonic properties of the samples. Monochromatic incident light with a well-defined wave vector $\mathbf{k}_i$ interacts with thermally activated acoustic phonons. The inelastically scattered light is detected at a fixed scattering angle. In combination with the given phonon wave vector $\mathbf{q}$, the sound velocity v can be calculated from the measured frequency shift f of the scattered light. The basic relation for the determination of the elastic stiffness tensor $\mathbf{c}=\{c_{kl}\}$, with $k,l=1,2,\ldots,6$, is the Christoffel equation (1)

$$\det\{l\mathbf{c}l^T-\mathbf{E}\rho[v(p,\mathbf{q})]^2\}=0 \tag{1}$$

with

$$l=\begin{bmatrix} l_1 & 0 & 0 & 0 & l_3 & l_2 \\ 0 & l_2 & 0 & l_3 & 0 & l_1 \\ 0 & 0 & l_3 & l_2 & l_1 & 0 \end{bmatrix}. \tag{2}$$

$\mathbf{c}$ is the fourth-rank elastic tensor of the sample written in shortened 6×6 Voigt notation, ρ is the mass density, and $v(p,\mathbf{q})$ is the velocity of a sound mode of polarization p that propagates with the wave vector $\mathbf{q}$. $\mathbf{E}$ is a 6×6 unit matrix. The l_i $(i=1,2,3)$ are the direction cosines of $\mathbf{q}$ with respect to the coordinate axes x_i. If acoustic losses are involved in the problem, the elastic tensor coefficients $c^*_{kl}=(c'_{kl}+ic''_{kl})$ become complex quantities and Eq. (1) holds strictly only if the condition $\mathbf{c}'\gg\mathbf{c}''$ between the real part $\mathbf{c}'$ and the imaginary part $\mathbf{c}''$ is fulfilled. In that case the measured sound velocity $v(p,\mathbf{q})$ is related to an elastic stiffness modulus via

$$c'(p,\mathbf{q})=\rho v^2(p,\mathbf{q})=\rho f^2(p,\mathbf{q})\Lambda^2\ , \tag{3}$$

where Λ denotes the phonon wavelength.

The acoustic polarization parameter p has three possible values for each $\mathbf{q}$ and in the most general case there exist one quasilongitudinal and two quasitransverse polarized modes. It is important to note that for NLC's the shear and quasishear stiffnesses vanish—or at least cannot be resolved—even at hypersonic frequencies where relaxation phenomena for (quasi)longitudinal modes are observed; therefore only the (quasi)longitudinal mode appears in the Brillouin spectra.

The principles of the experimental setup are shown in Fig. 2. A thin, filmlike sample (see Fig. 1) is illuminated by a laser beam of wavelength $\lambda_0=514.5$ nm. Usually

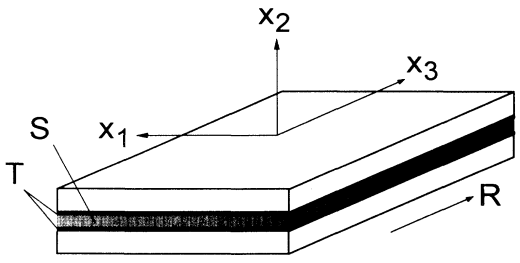

FIG. 1. Sample holder for PIM prepared sandwiches. The sample coordinate system is drawn too. R, rubbing direction; T, PIM coated sides of the glass plates; S, sample material.

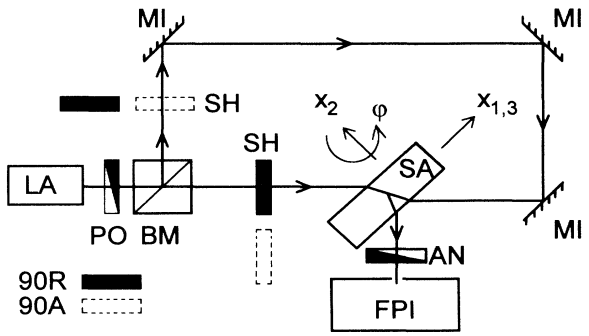

FIG. 2. Schematic setup of the Brillouin spectrometer. LA, argon ion laser; BM, beam splitter; PO, polarizer; AN, polarization analyzer; SH, shutter to select light path in order to realize 90A and 90R scattering geometries; SA, filmlike sample; MI mirrors; FPI, Fabry-Pérot interferometer and detection unit; x_1,x_2,x_3, sample coordinate system; φ, rotation angle for rotation around x_2.

the scattered light is detected at an outer scattering angle of 90°. Appropriate beam splitting and sample arrangements allow the realization of different scattering geometries and, as a consequence, phonon wave vectors of different directions and/or magnitudes. A five-pass or six-pass Fabry-Pérot interferometer analyzes the spectral components of the scattered light.

The directly measured quantities are the frequency shift f of the Brillouin line and its linewidth Γ (half width at half maximum) at fixed phonon wave vector $\mathbf{q}$, given by the chosen scattering geometry. In order to investigate the acoustic dispersion behavior of NLC's we realized several symmetry equivalent wave vectors of different magnitudes using the five appropriate scattering geometries schematically drawn in Fig. 3. Denoting the chosen scattering geometry by X, the related phonon wavelength $\Lambda(X)$ depends on the scattering conditions inside the sample and as a matter of fact also on the refractive indices involved (see Table III). Table III strictly holds only for samples of isotropic and cubic symmetries, but can be extended to lower symmetries with only small error, as long as moderate birefringences are involved in the scattering process [13].

The 90A and 90R scattering geometries are of special interest (Fig. 3); they are easy to adjust, they are perfectly suitable for Brillouin measurements on thin films, and they are complementary in order to yield the complete stiffness tensor of anisotropic samples from fiber symmetry to hexagonal symmetry. Using exclusively the 90A scattering geometry and turning the filmlike samples around an axis normal to its surface, a sound velocity curve can be measured as a function of the rotation angle φ (angle-resolving Brillouin spectroscopy), from which, by means of a nonlinear least-squares fit, several or, under favorable conditions, even all coefficients of the real part of the stiffness tensor can be calculated.

C. The optoacoustic dispersion function

Beyond the classical acoustic data, measurements combining the 90A and 90R scattering techniques may yield

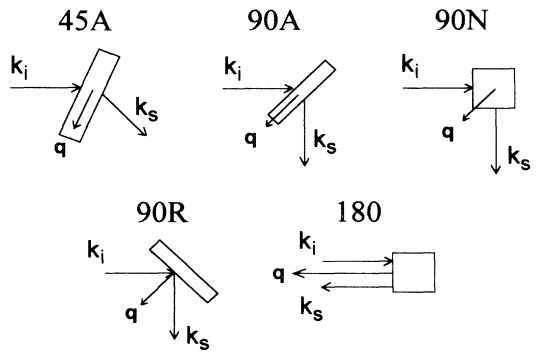

FIG. 3. Principles of the five used scattering geometries 45A, 90A, 90N, 90R, and 180. The directions of the incident light's wave vector $\mathbf{k}_i$, of the scattered light's wave vector $\mathbf{k}_s$ (both outside the sample), and of the phonon wave vector $\mathbf{q}$ are drawn. The outer scattering angle is determined by the angle between $\mathbf{k}_i$ and $\mathbf{k}_s$ and is indicated by the name of the scattering geometry.

TABLE III. Phonon wavelengths in the used scattering geometries. λ_0 laser wavelength (514.5 nm); X, scattering geometry; θ, outer scattering angle; θ^i, inner scattering angle; Λ, phonon wavelength; n, refractive index. It is important to note that Λ does not depend on n in the A geometries.

X	θ	θ^i	Λ
30A	30°	$2\arcsin\left[\frac{1}{n}\sin 15°\right]$	$\frac{\lambda_0}{2\sin(15°)}$
45A	45°	$2\arcsin\left[\frac{1}{n}\sin 22.5°\right]$	$\frac{\lambda_0}{2\sin(22.5°)}$
90A	90°	$2\arcsin\left[\frac{1}{n\sqrt{2}}\right]$	$\frac{\lambda_0}{\sqrt{2}}$
90N	90°	45°	$\frac{\lambda_0}{n\sqrt{2}}$
90R	90°	$180°-2\arcsin\left[\frac{1}{n\sqrt{2}}\right]$	$\frac{\lambda_0}{\sqrt{4n^2-2}}$
180	180°	180°	$\frac{\lambda_0}{2n}$

additional information on the acoustic dispersion behavior and on the optical properties of the sample. This information is given by the so-called optoacoustic dispersion function (D function [13]) and is purely based on sound frequencies measured in the 90A and 90R scattering geometries having symmetry equivalent phonon wave vectors (see e.g., Refs. [13,15]). As will be shown below, these additional facilities are of special importance for NLC's because, on the one hand, we can determine the magnitude of the nematic order parameter S [16] only from Brillouin measurements and, on the other hand, we can study broadly distributed and weakly activated acoustic relaxation processes even if sound attenuation and velocity data yield no reliable interpretation.

For the following discussion we define only those D functions which, based on the longitudinal sound modulus $c_{11}=c_{22}$, are the most suitable for NLC's with their inherent fiber symmetry (space group $D_{2h\infty}$),

$$D_i^{90R}|_{c_{11}}=\left[\frac{c'^{90R}_{11}}{c'^{90A}_{11}}(n_i^2-0.5)+0.5\right]^{1/2}. \tag{4}$$

From (4) it is evident that in the absence of acoustic dispersion, the refractive indices n_i ($i=1,3$) of our NLC samples can be deduced. Keeping in mind that x_1 and x_2 define symmetry equivalent directions ($n_1=n_2$), $n_i=D_i^{90R}|_{c_{11}}$, with $i=1,3$, can be evaluated from easily measurable sound frequencies using the following scattering conditions: (a) the 90A scattering geometry, with $\mathbf{q}$ along the x_1 axis and the electric field vectors of the incident and scattered light along the x_3 direction (according to Table III, Λ^{90A} is independent of the optical properties).

$$\Lambda^{90A}=\frac{\lambda_0}{\sqrt{2}}\ ; \tag{5}$$

(b) the 90R scattering geometry, with $\mathbf{q}$ directed along x_2 and the electric field vectors of the incident and scattered light along the x_1 and afterward along the x_3 direction yielding the acoustic wavelengths

$$\Lambda_i^{90R}=\frac{\lambda_0}{\sqrt{4n_i^2-2}} \quad \text{with } i=1,3\ . \tag{6}$$

Taking Eqs. (4)–(6) and denoting by $\hat{\mathbf{q}}$ a unit vector along $\mathbf{q}$, we obtain the desired relation between $D_i^{90R}|_{c_{11}}$ and the measured hypersonic frequencies $f^{90A}(\hat{\mathbf{q}}\|x_1)$ and $f_i^{90R}(\hat{\mathbf{q}}\|x_2)$, which yields the refractive indices n_i only from Brillouin data, provided that dispersion effects can be neglected:

$$D_i^{90R}|_{c_{11}}=\left[\frac{1}{2}\left[\frac{f_i^{90R}(\hat{\mathbf{q}}\|x_2)}{f^{90A}(\hat{\mathbf{q}}\|x_1)}\right]^2+\frac{1}{2}\right]^{1/2} \quad \text{with } i=1,3\ . \tag{7}$$

The difference $\Delta_i=(D_i^{90R}|_{c_{11}}-n_i)$ is a sensitive measure for dispersion effects. For a simple hypersonic relaxation process the temperature dependence of $D^{90R}|c_{11}$ and $n(T)$ is shown in Fig. 4(a). For relaxation processes $\Delta_i(T)\geq 0$ holds. This probe for acoustic dispersion is of special interest if (i) the phonon linewidths are difficult to measure or (ii) only the temperature dependence of the sound velocity and sound attenuation is available, but difficult to interpret. The latter case occurs as in our case, if one deals with a distributed and weakly activated relaxation process that is hard to resolve from the attenuation and velocity data. In order to demonstrate the power of this technique, we show in Fig. 4(b) the sound frequencies $f^{90R}(T)$, $f^{90A}(T)$ and the optoacoustic $D^{90R}(T)$ curves for the cubic phase of the orientational glass $K_xNa_{1-x}CN$ ($x=76$ mol %). It is interesting to note that although the sound frequencies of transverse polarized phonons $f^{90R}(T)$ and $f^{90A}(T)$ behave anomalously within the whole temperature regime, the $D^{90R}(T)$ curve reflects the refraction index $n(T)$ between 150 and 300 K. This means that the anomalous temperature behavior of the shear modulus c_{44} reflects no hypersonic dynamics, but c_{44} measures a purely static shear stiffness. Only below about 150 K do hypersonic relaxation processes occur in the frequency window of the measurement and thus cause the difference between the $D^{90R}(T)$ and the $n(T)$ function.

The birefringence Δn of our uniaxial NLC samples that is a good measure for the macroscopic order parameter is given by the difference ΔD ($\cong\Delta n$)

$$\Delta D=D_3^{90R}-D_1^{90R}\ . \tag{8}$$

The statement $\Delta D\cong\Delta n$ holds true [13] because of the small frequency differences between the quantities f_3^{90R} and f_1^{90R} that are only influenced by the refraction properties of the NLC's. Thus ΔD allows the determination of the sample's order parameter purely from Brillouin measurements. If there are only data available from 90R scattering geometry, ΔD may be estimated in good approximation from Eq. (7), even in case of acoustic relaxations by using an approximate value for n_1:

$$\Delta n\cong n_1\frac{[f_3^{90R}(\hat{\mathbf{q}}\|x_2)-f_1^{90R}(\hat{\mathbf{q}}\|x_2)]}{f_1^{90R}(\hat{\mathbf{q}}\|x_2)}\ . \tag{9}$$

The complex elastic tensor may be written as

$$c_{ij}^*=c_{ij}'-i\omega\eta_{ij}\ , \tag{10}$$

where η_{ij} is a viscosity tensor with the same symmetry properties as c'. In the case of damped acoustic modes the contribution to the spectral density $I(\mathbf{q},\omega)$ is proportional to the Fourier transform of a damped harmonic oscillator

$$I(\mathbf{q},\omega)\sim\frac{\gamma}{(2\gamma\omega)^2+(\omega_0^2-\omega^2)^2}\ , \tag{11}$$

where γ is the attenuation constant that may be formally

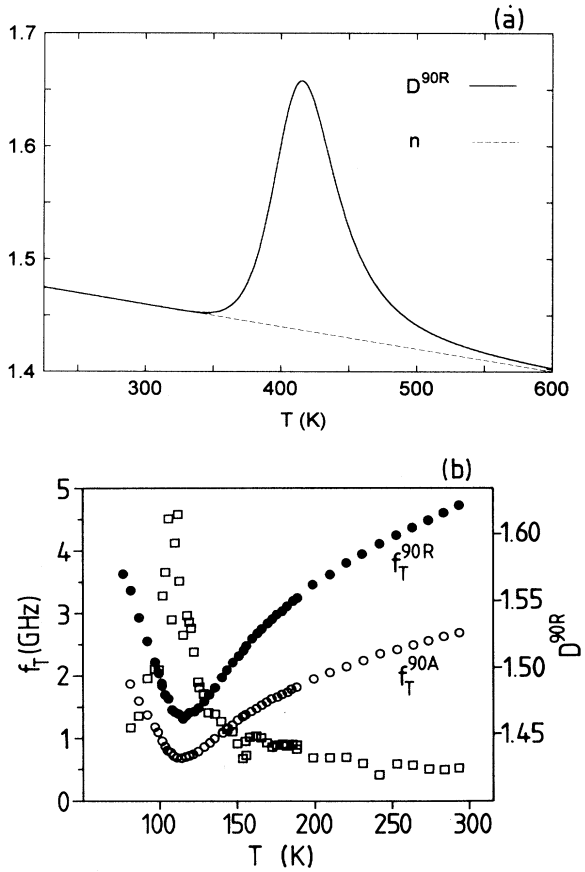

FIG. 4. (a) Temperature dependence of the refractive index n and of the optoacoustic dispersion function D^{90R} in the case of a strong relaxation process. (b) The example $K_{0.76}Na_{0.24}CN$ clearly demonstrates the power of the D function in characterizing hypersonic dispersion regimes. f_T^{90A} and f_T^{90R}, hypersonic frequencies of transverse polarized sound modes measured using the 90A and 90R scattering geometries, respectively; (□) D^{90R}, optoacoustic dispersion function. For further explanation see the text.

related to a viscosity coefficient

$$\gamma = \frac{q^2}{2\rho}\eta \ . \tag{12}$$

In the case that Brillouin lines of purely polarized and moderately attenuated acoustic modes are detected, a relation between the attenuation constant γ and the coefficients of the viscosity tensor $\boldsymbol{\eta}=\{\eta_{kl}\}$ is given by Eq. (12). Moreover, for moderate sound attenuation, $\gamma/2\pi$, given by Eq. (11), can be identified with the half width at half maximum Γ of our Brillouin lines.

D. Ultrasonics

There are also sound velocities and sound attenuation data presented in this work that have been measured using ultrasonic techniques. The ultrasound velocity measurements were performed at 1 MHz, using a variable-frequency resonance device. A detailed description of the method, the cell, and the precautions taken in order to ensure a high degree of sample purity can be found in Ref. [17]; only essential technical details are mentioned here. By use of stationary waves in a cylindrical cavity, this method enables the absolute value of the velocity to be measured from the position of the resonance peaks of the cavity. The cell was equipped with matched 3-MHz gold-plated quartzes, optically polished. The diameter of the sample ($\varnothing$=38 mm) was chosen to be larger than that of the ultrasonic beam ($\varnothing$=25 mm) in order to minimize possible parasitic effects due to the sidewalls. The interquartz length was 7.26 mm. This value was obtained by calibrating the cell with benzene, a test liquid of known properties. The temperature of the sample was controlled to within ± 0.01°C. The samples were oriented by a magnetic field of 10 kG.

It should be noted here that if one compares Brillouin results with ultrasonic measurements, the initial conditions are not the same. While Brillouin investigations are performed at a constant wave vector **q**, the frequency is the measured quantity and the sound velocity is therefore the phase velocity. In ultrasonic experiments the velocities of wave packets are measured, yielding the group velocity. The ultrasonic absorption coefficient α is connected to the related viscosity coefficient in a first approximation by

$$\frac{\alpha}{f^2} = \frac{2\pi^2}{\rho v^3}\eta \ , \tag{13}$$

where f denotes the ultrasonic frequency and v the measured group velocity both specified for a given sound mode [18].

III. RESULTS AND DISCUSSION

Despite the continuously broken rotational symmetry in nematics, there is no anisotropy observed for the real part of the elastic moduli at low frequencies (see, e.g., Refs. [1,4]). However, hydrodynamic theories of the nematic state allow for anisotropic acoustic attenuation because of the symmetry properties of the relevant transport coefficients, i.e., the viscosity tensor and the thermal conductivity tensor. The nematic symmetry is characterized by a preferential direction of the molecules' axes, called the director **n**. The director field induces restoring forces described by the Frank elastic constants [3]. These may be measured in low frequency experiments because of the lack of any static shear stiffness in nematics. It can be shown, however, that their influence on second-order elastic constants may be neglected since they contribute only in the fourth order of **q** to the elastic dispersion relation. At hypersonic wavelengths this results in contributions to the elastic stiffness moduli of the form Kq^2, where K is a Frank elastic constant of a typical order of 10^{-11} N, and typical wave numbers in a Brillouin experiment are of the order 10^7 m^{-1}. Henceforth this contribution is of the order of 10^{-6} compared with the compression modulus [19] and therefore cannot be resolved by classical Brillouin techniques.

Ultrasonic data confirm the above prediction of an isotropic elastic stiffness behavior for most NLC's (see Refs. [20,21] and Figs. 5 and 6). However, there were some materials in which a small elastic stiffness anisotropy of far less than 1% could be shown [22]. This anisotropy effect was attributed by Jähnig [23] to trans-gauche relaxation processes in the molecules' alkylic end groups (see, e.g., Ref. [24]) and, as a matter of fact, is more evident in the related sound attenuation data [7,23].

Brillouin measurements on different NLC's have shown (e.g., Refs. [12,25] and Figs. 5–7) that the hypersound velocity of NLC's is usually significantly larger than ultrasound velocities measured at the same temperature within the nematic state. This sound velocity difference persists also in the adjacent isotropic phase and was first reported by Clark and Liao [12] for MBBA. Their Brillouin measurements were performed by technical reasons only in the isotropic phase. Thus they had no information about the anisotropy of the nematic state. In order to measure closer to ultrasonic frequencies, Harada and Crooker performed Brillouin spectroscopy on MBBA within the isotropic phase using the 30A scattering

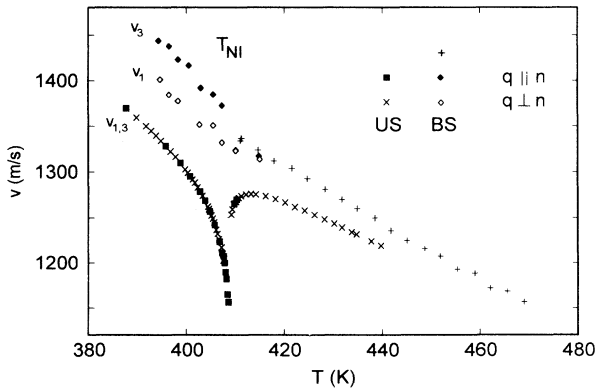

FIG. 5. Sound velocity of PAA in the oriented nematic and the isotropic state. Upper curve, Brillouin measurement at about 3.9 GHz, 90A-scattering geometry; lower curve, ultrasonic measurement at 1 MHz, T_{NI}, nematic-isotropic phase transition. In the oriented nematic state phonon propagation along and perpendicular to the director **n** has been investigated.

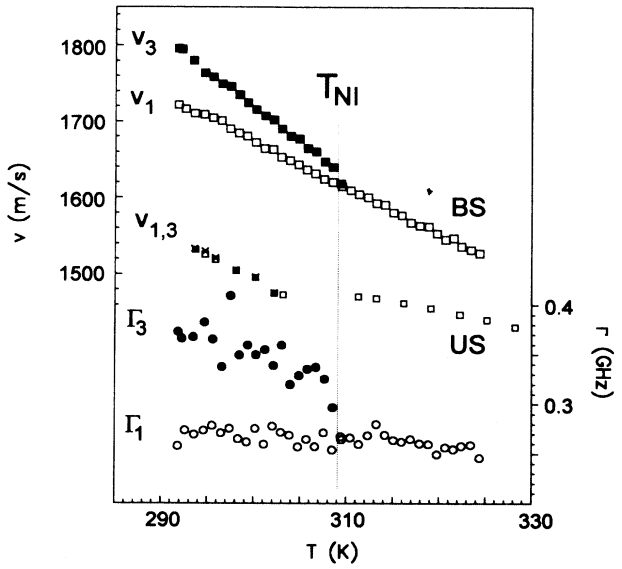

FIG. 6. Temperature-dependent sound velocity of 5CB. US, ultrasonic measurement at 1 MHz. (□) v_3 (**q**∥**n**); (×) v_1 (**q**⊥**n**). BS, Brillouin measurement at about 4.5 GHz. v_3 (**q**∥**n**), sound propagation along the director; v_1 (**q**⊥**n**), sound propagation perpendicular to the director. Γ_3 and Γ_1 are the related hypersound attenuations. T_{NI}, nematic-isotropic phase transition temperature.

geometry [25]. An important point of their paper from our point of view was the compilation of viscosity data covering a wide frequency range at a fixed temperature difference $T-T_{NI}=5$ K. (In order to compare data of MBBA obtained by different researchers, this renormalization of the temperature scale is necessary since T_{NI}

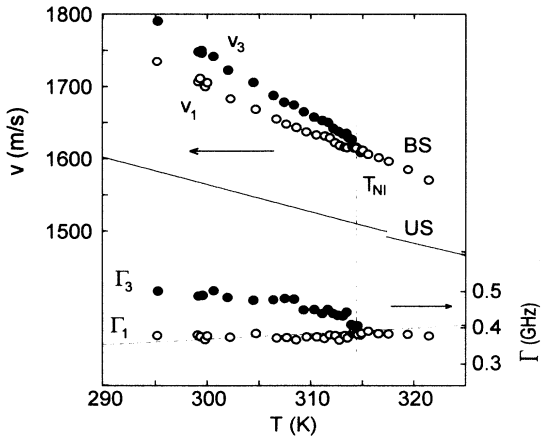

FIG. 7. Temperature-dependent sound velocity of MBBA. Brillouin measurement (BS) using 90A scattering geometry and also ultrasonic data (US) measured at 23.07 MHz (from Ref. [28]). Lower curve, hypersonic linewidth Γ. The indicated curve results from a model calculation to simulate the temperature behavior of Γ (see text). v_3, Γ_3, sound propagation along the director; v_1,Γ_1, sound propagation perpendicular to the director, T_{NI}, nematic-isotropic phase transition temperature. In the ultrasonic measurement the phase transition was found at a slightly higher temperature.

strongly depends on the content of adsorbed water. It has been assumed, however, by Harada and Crooker and confirmed by our experiences that viscoelastic properties in a first approximation only depend on the difference $T-T_{NI}$ and not on the absolute temperature itself.) Their data analysis led them to a conclusion already proposed by Clark and Liao [12] that there should be a pronounced relaxation process with a main relaxation within the low gigahertz range, which is the typical frequency domain of Brillouin spectroscopy. Moreover, they claimed that this relaxation process is not due to the trans-gauche relaxations of the alkyl chains, but reflects an additional relaxation process. PAA contains no alkyl chains within the molecules, but shows a drastically increased hypersonic velocity anisotropy of the same order as that found for NLC's with alkyl chains, as we could show clearly by our comparative ultrasonic and Brillouin investigations (Fig. 5). Thus the hypothesis of Harada and Crooker [25] is confirmed. It is likely that the strong hypersonic anisotropies found for virtually all NLC's (Refs. [8–11] and Figs. 5–7) are a consequence of this hypersonic relaxation process too, which in turn indicates that universal nature of this process (see below).

Having in mind the existence of a rather universal hypersonic relaxation process in NLC's, it was amazing that Brillouin measurements made as a function of temperature on MBBA [14], n-CB [8,26], 4-(n-heptyloxy)-4′-cyanobiphenyl (7OCB) [10,27], 4-(n-octyloxy)-4-cyanobiphenyl (8OCB) [8] gave no hints at all for the presence of a relaxation process within the temperature and frequency window under study. The hypersonic velocities $v(T)$ as well as the Brillouin linewidths $\Gamma(T)$ behave as they would do due to usual anharmonicity. Careful reinvestigations on MBBA and 5CB have confirmed this result. As shown by Fig. 7, the hypersonic velocity and attenuation of MBBA given by the $v(T)$ and $\Gamma^{90A}(T)$ curves behave completely flat in the nematic as well as in the isotropic phase and give particularly no hint for an attenuation maximum. Therefore, as a first working hypothesis we assumed that the Brillouin data for all investigated materials correspond to the slow motion regime of the predicted relaxation process even at the highest measured temperatures. This working hypothesis implies that (i) the described relaxation process is active only in the frequency range between about 20 MHz and about 1 GHz, which means that it is active only between typical ultrasound and Brillouin frequencies, and as a consequence (ii) the optoacoustic $D^{90R}(T)$ function (see Sec. II C) coincides with the related refractive index function $n(T)$.

In order to check this hypothesis we determined the $D^{90R}(T)$ curves for certain NLC's. While in the dispersionless case $D^{90R}(T)$ reflects the temperature behavior of the refractive index $n(T)$, it exceeds $n(T)$ in the relaxation regime (see Sec. II C, Fig. 4). For MBBA we performed $n(T)$ measurements using an Abbé refractometer compensated for our laser wavelength of $\lambda_0=514.5$ nm [Fig. 10(a)]. In order to determine $D^{90R}(T)$ of 5CB [Fig. 10(b)] we used $f^{90R}(T)$ data from Ref. [26]. Related $n(T)$ values were extrapolated from data given in Ref. [35] for the nematic phase and for our laser wavelength

$\lambda_0 = 514.5$ nm. To obtain $n(T)$ data for the isotropic phase, we calculated the orientation average

$$\langle n(T) \rangle = \tfrac{1}{3}[2n_1(T) + n_3(T)] \quad (14)$$

for the nematic phase and extrapolated $\langle n(T) \rangle$ to temperatures $T > T_{NI}$ (Fig. 10). Special care has been taken to avoid systematic errors that could affect the absolute accuracy. For 5CB as well as for MBBA there is an obvious vertical shift of $D^{90R}(T)$ versus $n(T)$, which indicates clearly the presence of a relaxation process over the whole frequency-temperature window studied. These results are obviously in contradiction to the working hypotheses (i) and (ii) made above. Moreover, the fact that the $D^{90R}(T)$ curves are almost constantly shifted in comparison with the related $n(T)$ curves suggests small activation energies of the relaxation processes involved. As a consequence the relaxation regime seems to extend over hundreds of degrees Kelvin.

In order to verify whether the relaxation process suggested first by Clark and Liao [12] for MBBA has its main relaxation frequency really in the center of the Brillouin frequency regime, we performed Brillouin measurements on MBBA using the 45A, 90A, 90R, 90N, and 180 scattering geometries. It should be stressed that a stringent test of the relaxation hypothesis requires a simultaneous data analysis of the real and imaginary parts of the complex elastic moduli as a function of frequency. To do this we took into account the viscosity data compiled by Harada and Crooker [25], related sound velocity data from the literature [12,25,28–30], our own Brillouin data, and recent Brillouin results of Lerman, Sabirov, and Utarova [31] (unfortunately, the latter publication contains no attenuation data). A simultaneous fit to both sound velocity and viscosity data was performed using a model function assuming that the longitudinal elastic stiffness of MBBA undergoes two Debye-like relaxation processes (Fig. 8). Therefrom the frequency behavior of sound velocity and viscosity can be calculated. A slight complication occurs from the fact that in MBBA at 5 K above T_{NI} the critical process and the alkyl chain relaxation overlap. In order to account for this we allowed for a distribution parameter β for the low frequency process. As far as the hypersonic process is concerned, it showed, however, that neither a distribution parameter nor additional relaxation processes could improve the fit result.

It turns out that the fit only roughly describes the sound velocity and viscosity data. For the wave vector $\mathbf{q}^{45A}$ our own Brillouin data deviate systematically from the fit curve, indicating a possibly different evolution of the hypersonic relaxation process, as shown by the fit curves in Fig. 8. Taking into account that the uncertainty for our sound velocity data is certainly less than 0.5%, these fit curves give only a qualitative estimation of the true situation. This results particularly from the fact that our sound velocity data are partly incompatible with those of Ref. [31]. A careful check of our Brillouin data did not elucidate the systematic deviations between the data of Lerman, Sabirov, and Utarova [31] and ours.

Beside experimental inconsistencies, physical incompatibilities may result from the fact that ultrasonic measurements yield the group velocity $v_g = \partial\omega/\partial q$, whereas in Brillouin measurements the phase velocity $v_{ph} = \omega/q$ is measured. According to Evans and Powles [32], v_g and v_{ph} have to be distinguished in a relaxation regime. In order to check possible influences on the Brillouin data given in Fig. 8 due to differences between v_g and v_{ph} we fitted our measured hypersonic frequencies as a function of wave number using a linear and a quadratic function, respectively [Fig. 9(a)]. From the distribution of the residuals it is clear that the $\omega(q)$ curve can be approximated quite well by a second-order polynomial. In Fig. 9(b) the calculated phase velocity v_{ph} and the group velocity v_g are shown as functions of wave number q. In a worst case the difference between both quantities arises up to 5% at the highest values of q. This shows that the hypersonic velocity data would not be renormalized significantly if inherent differences between phase and group velocities were taken into account.

Summarizing the arguments given above, we conclude that even if between ultrasonic and hypersonic frequencies the true relaxation curves deviate to a certain extent from what is shown in Fig. 8, it is obvious that the Brillouin data measured at $T_{NI}+5$ K yield a relaxation step in the frequency window of the Brillouin technique.

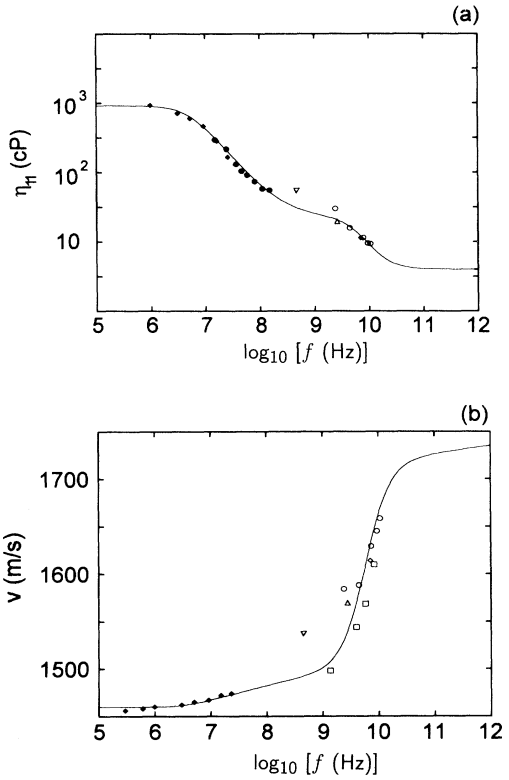

FIG. 8. Compilation of all available data of (a) viscosity and (b) sound velocity of MBBA at $T_{NI}+5$ K. Filled symbols, ultrasonic measurements (● from Ref. [28], ♦ from Ref. [29]). Open symbols, Brillouin measurements (∇ from Ref. [30], Δ from Ref. [25], ◇ from Ref. [12], □ from Ref. [31], ○ from this work). The curve is a nonlinear least-squares fit, simultaneously in viscosity and sound velocity. For further details see the text.

Moreover, the high frequency end of the dispersion step is not reached yet at the highest investigated frequencies. The main relaxation frequency from the fit is $f_r = 6.5 \pm 3.0$ GHz.

Taking into account the presence of a universal relaxation step above ultrasonic frequencies and in addition a significant acoustic anisotropy at hypersonic frequencies found in the nematic state of all NLC's, the question appears to find a sufficiently general mechanism that is responsible for explaining the observations. Clark and Liao proposed a relaxation of the vibrational specific heat as it was discussed for benzene [33]. However, usually it is assumed that longitudinal polarized high frequency sound waves cause more or less adiabatic compression. Periodic heating and cooling occurs with the consequence of heat flow. The related contribution to the sound attenuation yields a background attenuation described by

$$\left[\frac{\alpha}{f^2}\right]_{\text{th}} = \frac{2\pi^2}{\rho v^3}(\gamma - 1)\frac{\kappa}{C_p} , \tag{15}$$

where κ is the thermal conductivity, γ the adiabatic exponent, and C_p the specific heat at constant pressure. By reason of magnitude, the term given by Eq. (15) may usually be neglected versus structural viscosity contributions. If this is not the case, a formal argument allows the introduction of a so-called "thermal viscosity" η_{th} in order to formulate the analogy to the expressions for viscous losses. If the above mentioned argument holds true, it follows that the observed hypersonic relaxation process is due to a predominant coupling between the longitudinal acoustic deformation field $\varepsilon_{33}(\mathbf{r},t)$ and the appropriate internal thermodynamic variables which yield heat flow properties that relax at hypersonic frequencies. Collisions of molecules enable the interchange of energy between translational and vibrational degrees of freedom. The time constant for the relaxation into equilibrium between these types of motion is, however, much larger than the time to reach an equilibrium between different vibrational degrees of freedom because of the necessary collisions. This should result into a classical Debye relaxation process to be seen in the specific heat and in the thermal conductivity, respectively, that is characterized by a single relaxation time constant τ. Thus both C_p and η_{th} become complex quantities and thus yield a relaxing contribution to the hypersonic velocity and attenuation. A good overview about this kind of mechanisms is given, e.g., by the review of Lamb [34]. The formal analogy between sound attenuation due to viscous and/or thermal losses shows that a measurement of a dispersion step in the complex elastic properties does not allow us to discriminate between the structural or thermal origin. An argument in favor of a thermal induced hypersonic relaxation process is the common behavior of chemically very different liquid crystal molecules, which may not easily be related to some structural relaxations.

Typical values for the activation energies of thermal relaxation processes are about $E_a/k \approx 500$ K [34]; moreover, thermal relaxations are expected to follow an Arrhenius law. This assumption, together with the knowledge of the relaxation frequency at a fixed temperature, enabled us to simulate roughly the contribution of the relaxation process to the hypersonic attenuation constant Γ^{90A} as a function of temperature (curve in Fig. 7). We stress the fact that no contribution to sound attenuation other than the dispersion mechanism has been considered in the calculation; the value of Γ^{90A} at the tem-

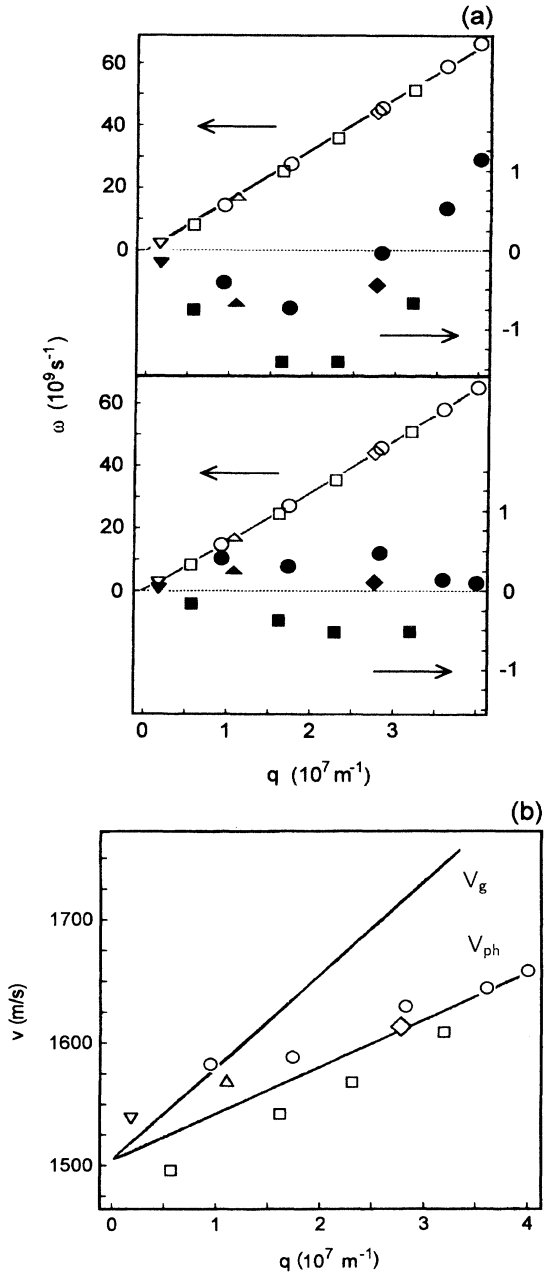

FIG. 9. (a) Open symbols, dispersion relation of MBBA as measured by Brillouin spectroscopy, fitted using a straight line (upper picture) and a second-order polynomial (lower picture). The corresponding absolute residuals (filled symbols) are given too. (b) Difference of v_{ph} and v_g as functions of wave number q as calculated under the assumption of a parabolic dispersion relation (see text).

perature $T_{NI}+5$ K was taken from our data. Although we made a rather rough assumption for our estimation, the calculated $\Gamma^{90A}(T)$ curve agrees quite well with the measured data. Especially the flat behavior of the measured $\Gamma^{90A}(T)$ curve seems therefore to be in agreement with the assumed relaxation process.

We have not discussed yet the significance of the hypersonic relaxation process for the elastic anisotropy found at gigahertz frequencies within the nematic phase of NLC's. As shown in Figs. 5–7 and Table IV the acoustic anisotropy found at Brillouin frequencies for chemically quite different NLC's are very close. This supports the idea that the hypersonic anisotropy of NLC's is based on the same relaxation mechanism as the relaxation step in the isotropic phase of these materials. Unfortunately, it is not yet clear how this relaxation process is modified at the first-order transition from the isotropic to the nematic state. Of course, due to the symmetry breaking event at T_{NI}, morphic thermodynamic and transport coefficients appear and may affect the thermal relaxation process. The longitudinal relaxation frequency f_r found for the isotropic state is likely to become different for different directions of phonon propagation; they may even change their time scales. However, due to the fact that within the nematic state c_{33} as well as c_{11} measured at Brillouin frequencies significantly exceed the related values measured at ultrasonic frequencies and furthermore that $D_i^{90R}(T)$ of 5CB (with $i=1,3$) exceeds $n_i(T)$ (Fig. 10, extrapolated from Ref. [35]), we conclude that these Brillouin data are also within the relaxation regime. It appears also from Fig. 10 that the relation $\Delta D^{90R}\sim\Delta n$ (Sec. II C) is fulfilled.

At low frequencies the unified hydrodynamic theory [4] for NLC's allows for anisotropic transport coefficients, but not for anisotropic elastic moduli. The classical hydrodynamic behavior is conserved more or less up to ultrasonic frequencies; the onset of the nematic order parameter apparently does not break the elastic isotropy at these frequencies. Only in the hypersonic frequency regime, where the order parameter fluctuations are already clamped, is the elastic anisotropy degeneracy removed. Because of the thermal relaxation process the transport coefficients become complex quantities and thereby contribute to an anisotropic real part of the elastic modulus. Furthermore, the amplitudes and the relaxation time constants of the relaxation process may be different for different symmetry directions, which, at least in principle, results in different longitudinal moduli and reflects thus the broken symmetry.

In this context we compared the evolution of hypersonic anisotropy with the magnitude of the nematic order parameter. As usual, the latter was taken to be proportional to ΔD^{90R}. As a model substance we used again MBBA. According to Moseley [36], the elastic anisotropy has been described by the following "orientation" parameter

$$P_2^M=\frac{c_{33}-c_{\rm iso}}{c_{33}}\approx\frac{c_{33}-c_{11}}{c_{33}}\ , \tag{16}$$

where $c_{\rm iso}$ represents the longitudinal modulus of the macroscopically disordered (polydomain) nematic state which has been approximated by c_{11}. Corresponding values for P_2^M and ΔD^{90R} were taken from our measurements. Taking into account the first-order character of the nematic-isotropic transition, the values ΔD_0 and $(P_2^M)_0$ in Fig. 11 give the onset values at T_{NI}. The continuous line in Fig. 11 was obtained from a least-squares fit of the second-order polynomial

$$P_2^M=a[\Delta D^{90R}-\Delta D_0(T_{\rm NI})]^2+(P_2^M)_0 \tag{17}$$

to the experimental results. It turns out that there exists

TABLE IV. Anisotropies of the different samples in the nematic phase as measured by Brillouin spectroscopy (from Ref. [26]).

Material	$\Delta v/v$ (%)	T (K)	$T_{NI}-T$ (K)
PAA	3.7	394	14.7
MBBA	2.8	304	14.2
5CB	3.8	294	14.7

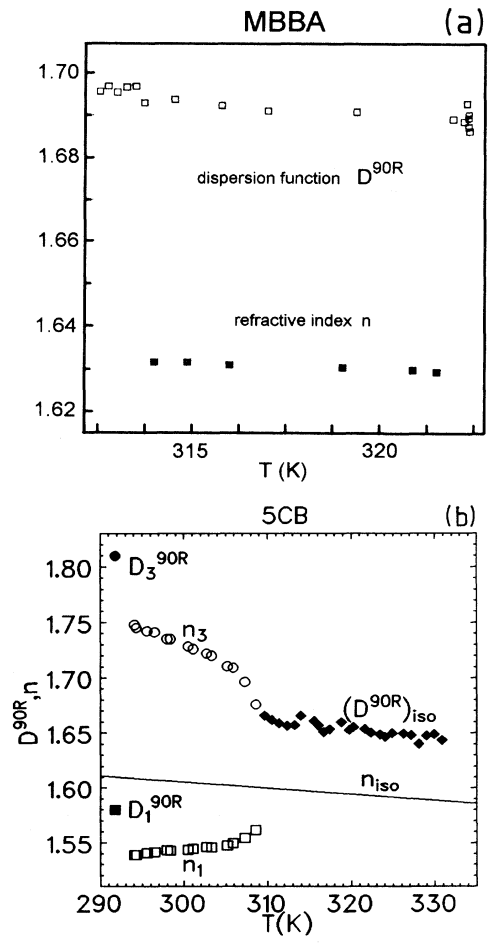

FIG. 10. Optacoustic dispersion function D^{90R} and refractive index n as functions of temperature T. (a) MBBA: □, D^{90R}; ■, refractive index n. (b) 5CB: ●, D_3^{90R}; ■, D_1^{90R}; ○, n_3; □, n_1 (n_1 and n_3 extrapolated from Ref. [35]); straight line, $n_{\rm iso}$; ◆, D^{90R} in the isotropic phase. For further explanation see the text.

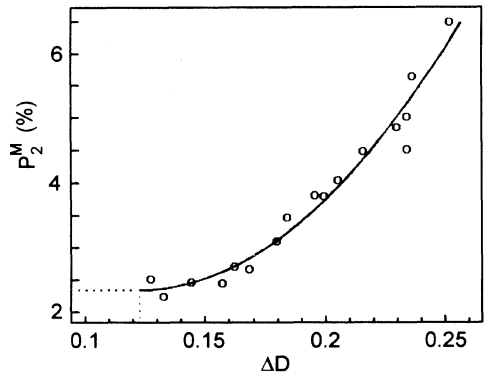

FIG. 11. Orientation parameter P_2^M of MBBA as a function of the macroscopic nematic order parameter given by the function ΔD. For further explanation see the text.

a quadratic correlation between the order parameter and the hypersonic anisotropy parameter P_2^M which is not found at lower frequencies. An interpretation of this result in terms of a Landau ansatz [37–39] including dynamic effects will be given elsewhere [40].

IV. CONCLUSIONS

We investigated the ultrasonic and hypersonic second-order elastic properties of several classical liquid crystals with the following results. Ultrasonic experiments show a critical slowing down of the longitudinal sound velocity below and above the nematic-isotropic phase transition while Brillouin experiments do not. Concerning order parameter fluctuations, the hypersonic velocity is measured in the slow motion regime. Ultrasonic measurements show no or nearly no sound velocity anisotropy in the nematic phase, while Brillouin experiments generally do, as it has been confirmed clearly now. Over the whole temperature range the ultrasonic measurements yield lower absolute sound velocities than the Brillouin experiments. These differences are discussed for quite a while in terms of a high frequency relaxation process. By extending the available frequency range to the highest frequencies measurable by Brillouin spectroscopy of acoustic modes we improved the available data base for MBBA. The simultaneous comparison of the real and imaginary parts of the elastic modulus as a function of frequency by making use of all available data clearly strengthens the hypothesis of an underlying relaxation process. The interpretation as a thermal relaxation process as previously assumed is worked out in some detail. The temperature behavior of the optoacoustical dispersion function D^{90R} proves the relaxation hypothesis. From the behavior of D_1^{90R} and D_3^{90R} in comparison with n_1 and n_3 in the nematic state of 5CB, we claim that the hypersonic relaxation mechanism is not renormalized significantly at the nematic-isotropic transition. The universality of the process for most nematic liquid crystals is pointed out by the qualitative and quantitative similarity of the presented data for all investigated material classes, especially for those with alkylic chains and those without alkylic chains. The technique of Brillouin refractometry has been developed as a powerful tool to yield reliable information about broadly distributed and weakly activated acoustic relaxation processes even if sound attenuation and velocity data alone do not. At hypersonic frequencies a quadratic dependence between the order parameter and the hypersonic anisotropy parameter P_2^M was found that does not exist at lower frequencies.

ACKNOWLEDGMENT

We are indebted to Dr. P. Martinoty for many discussions about the ultrasonic and relaxation aspects of the presented data.

[1] P. G. De Gennes, *The Physics of Liquid Crystals* (Clarendon, Oxford, 1974).
[2] D. Forster, *Hydrodynamic Fluctuations, Broken Symmetries and Correlation Functions* (Benjamin, London, 1975).
[3] C. W. Oseen, Trans. Faraday Soc. **29**, 883 (1933); H. Zocher, *ibid.* **29**, 945 (1933); F. C. Frank, Discuss. Faraday Soc. **25**, 19 (1958).
[4] P. C. Martin, O. Parodi, and P. S. Pershan, Phys. Rev. A **6**, 2401 (1972).
[5] F. Jähnig, Z. Phys. **258**, 199 (1973).
[6] K. Miyano and J. B. Ketterson, Phys. Acoust. **14**, 93 (1979).
[7] S. Candau, P. Martinoty, and R. Zana, J. Phys. (Paris) Lett. **36**, L13 (1975).
[8] G. W. Bradberry and C. F. Clarke, Phys. Lett. **95A**, 305 (1983).
[9] G. W. Bradberry and J. M. Vaughan, Phys. Lett. **62A**, 225 (1977).
[10] J. K. Krüger, in *Optical Techniques to Characterize Polymer Systems,* edited by H. Bässler (Elsevier, Amsterdam, 1989).
[11] D. G. Gleed, J. R. Sambles, and G. W. Bradberry, Phys. Lett. A **134**, 440 (1989).
[12] N. A. Clark and Y. Liao, J. Chem. Phys. **63**, 4133 (1975).
[13] J. K. Krüger, A. Marx, L. Peetz, R. Roberts, and H.-G. Unruh, Colloid Polym. Sci. **264**, 403 (1986).
[14] J. K. Krüger, R. Kimmich, J. Sandercock, and H. G. Unruh, Polym. Bull. **5**, 615 (1981).
[15] J. K. Krüger, L. Peetz, R. Siems, H.-G. Unruh, M. Eich, O. Herrmann-Schönherr, and J. H. Wendorff, Phys. Rev. A **37**, 2637 (1988).
[16] V. Zwetkoff, Acta Physicochim. (USSR) **16**, 132 (1942).
[17] D. Collin J. L. Gallani, and P. Martinoty, Phys. Rev. A **34**, 2255 (1986).
[18] B. A. Auld, *Acoustic Fields and Waves in Solids* (Wiley, New York, 1973).
[19] R. Lahmer, Diplomarbeit, Saarbrücken, 1992.
[20] K. A. Kemp and S. V. Letcher, Phys. Rev. Lett. **27**, 1634 (1971).

[21] E. D. Liebermann, J. D. Lee, and F. C. Moon, Appl. Phys. Lett. **18**, 280 (1971).
[22] A. E. Lord and M. M. Labes, Phys. Rev. Lett. **25**, 570 (1970).
[23] F. Jähnig, Chem. Phys. Lett. **23**, 262 (1973).
[24] S. Nagai, P. Martinoty, S. Candau, and R. Zana, Mol. Cryst. Liq. Cryst. **31**, 243 (1975).
[25] T. Harada and P. P. Crooker, Mol. Cryst. Liq. Cryst. **42**, 283 (1977).
[26] J. K. Krüger, C. Grammes, R. Jiménez, J. Schreiber, K.-P. Bohn, J. Baller, C. Fischer, D. Rogez, C. Schorr, and P. Alnot, Phys. Rev. E (to be published).
[27] C. Grammes, Dissertation, Saarbrücken, 1993.
[28] D. Eden, C. W. Garland, and R. C. Williamson, J. Chem. Phys. **58**, 1861 (1973).
[29] P. Martinoty and S. Candau, C. R. Acad. Sci. Paris **271**, 107 (1970).
[30] T. R. Steger and J. D. Litster, Liq. Crvst. Ordered Fluids **2**, 671 (1974).
[31] V. U. Lerman, L. M. Sabirov, and T. M. Utarova, Zh. Eksp. Teor. Fiz. **104**, 2366 (1993) [JETP **77**, 55 (1993)].
[32] W. A. B. Evans and J. G. Powles, J. Phys. A **7**, 1944 (1974).
[33] J. L. Hunter, E. F. Carome, H. D. Dardy, and J. A. Bucaro, J. Acoust. Soc. Am. **40**, 313 (1966).
[34] J. Lamb, Phys. Acoust. **2**, 203 (1965).
[35] P. P. Karat and N. V. Madhusudana, Mol. Cryst. Liq. Cryst. **36**, 51 (1976).
[36] W. W. Moseley, J. Appl. Polym. Sci. III **9**, 266 (1960).
[37] L. D. Landau and E. M. Lifschitz, *Lehrbuch der Theoretischen Physik V* (Akademie-Verlag, Berlin, 1975).
[38] L. D. Landau and I. M. Khalatnikov, Dokl. Akad. Nauk. SSSR **96**, 469 (1954).
[39] W. Rehwald, Adv. Phys. **22**, 721 (1973).
[40] J. K. Krüger, C. Grammes, and A. Dvorak (unpublished).